RESEARCH ARTICLE

JBMR®

Mineral Crystal Thickness in Calcified Cartilage and Subchondral Bone in Healthy and Osteoarthritic Human Knees

Mikko A.J. Finnilä,[1,2] Shuvashis Das Gupta,[1] Mikael J. Turunen,[3] Iida Hellberg,[1] Aleksandra Turkiewicz,[4] Viviane Lutz-Bueno,[5] Elin Jonsson,[4] Mirko Holler,[5] Neserin Ali,[4] Velocity Hughes,[4] Hanna Isaksson,[6] Jon Tjörnstrand,[7] Patrik Önnerfjord,[8] Manuel Guizar-Sicairos,[5] Simo Saarakkala,[1,9] and Martin Englund[4]

[1]Research Unit of Medical Imaging, Physics and Technology, Faculty of Medicine, University of Oulu, Oulu, Finland
[2]Medical Research Center, University of Oulu, Oulu, Finland
[3]Department of Applied Physics, Faculty of Science and Forestry, University of Eastern Finland, Kuopio, Finland
[4]Clinical Epidemiology Unit, Orthopaedics, Department of Clinical Sciences Lund, Faculty of Medicine, Lund University, Lund, Sweden
[5]Paul Scherrer Institut, Villigen PSI, Switzerland
[6]Department of Biomedical Engineering, Lund University, Lund, Sweden
[7]Department of Orthopaedics, Skåne University Hospital, Lund, Sweden
[8]Rheumatology and Molecular Skeletal Biology, Department of Clinical Sciences Lund, Faculty of Medicine, Lund University, Lund, Sweden
[9]Department of Diagnostic Radiology, Oulu University Hospital, Oulu, Finland

ABSTRACT

Osteoarthritis (OA) is the most common joint disease, where articular cartilage degradation is often accompanied with sclerosis of the subchondral bone. However, the association between OA and tissue mineralization at the nanostructural level is currently not understood. In particular, it is technically challenging to study calcified cartilage, where relevant but poorly understood pathological processes such as tidemark multiplication and advancement occur. Here, we used state-of-the-art microfocus small-angle X-ray scattering with a 5-μm spatial resolution to determine the size and organization of the mineral crystals at the nanostructural level in human subchondral bone and calcified cartilage. Specimens with a wide spectrum of OA severities were acquired from both medial and lateral compartments of medial compartment knee OA patients ($n = 15$) and cadaver knees ($n = 10$). Opposing the common notion, we found that calcified cartilage has thicker and more mutually aligned mineral crystals than adjoining bone. In addition, we, for the first time, identified a well-defined layer of calcified cartilage associated with pathological tidemark multiplication, containing 0.32 nm thicker crystals compared to the rest of calcified cartilage. Finally, we found 0.2 nm thicker mineral crystals in both tissues of the lateral compartment in OA compared with healthy knees, indicating a loading-related disease process because the lateral compartment is typically less loaded in medial compartment knee OA. In summary, we report novel changes in mineral crystal thickness during OA. Our data suggest that unloading in the knee might be involved with the growth of mineral crystals, which is especially evident in the calcified cartilage. © 2022 The Authors. *Journal of Bone and Mineral Research* published by Wiley Periodicals LLC on behalf of American Society for Bone and Mineral Research (ASBMR).

KEY WORDS: OSTEOARTHRITIS; ANALYSIS/QUANTITATION OF BONE; MATRIX MINERALIZATION; BONE MODELING AND REMODELING; COLLAGEN

Introduction

In large joints, rigid bone provides a structural foundation for smooth articular cartilage that enables almost frictionless movement. The most important constituents of articular cartilage are proteoglycans and collagens, mainly of type II. Charged proteoglycans attract ions, which generate osmotic pressure and thus, have a crucial role in maintaining the dynamic compressive

Received in original form July 13, 2021; revised form May 17, 2022; accepted June 26, 2022.
Address correspondence to: Mikko A.J. Finnilä, PhD, Research Unit of Medical Imaging, Physics and Technology, Faculty of Medicine, University of Oulu, POB 5000, FI-90014 Oulu, Finland. E-mail: mikko.finnila@oulu.fi
Additional Supporting Information may be found in the online version of this article.
SS and ME contributed equally to this work.
Journal of Bone and Mineral Research, Vol. 37, No. 9, September 2022, pp 1700–1710.
DOI: 10.1002/jbmr.4642

properties of cartilage.[1,2] Fibrillar collagen is organized in a pattern also known as "Benninghoff arcades" and it provides tensile strength for the cartilage.[3] These properties allow cartilage to dissipate as well as distribute various types of loadings evenly on underlying mineralized tissues.[4,5] The subchondral bone is composed of type I collagen fibrils embedded with hydroxyapatite crystals, contributing to the toughness and stiffness of the tissue.[6-8] The subchondral bone should be rigid enough to transfer mechanical load but elastic enough to reduce high stress in articular cartilage.[9] Furthermore, bone is a metabolically active tissue that can adapt to mechanical loading, and it has been identified as a viable target tissue for pharmaceutical therapies.[10]

Calcified cartilage forms an interface between the subchondral bone and articular cartilage. A thin basophilic line in histological sections is known as tidemark, which forms the interface between the articular cartilage and calcified cartilage.[11] There is another highly mineralized interface between calcified cartilage and subchondral bone called the cement line.[12] Calcified cartilage resembles both tissues by consisting of a cartilage-like organic matrix with proteoglycans embedded in a type II collagen network, which is mineralized as the bone tissue.[13,14] However, calcified cartilage has been reported to have a higher degree of mineralization than subchondral bone,[15] whereas its stiffness has been estimated to fall between articular cartilage and underlying subchondral bone.[16] Accordingly, it has been suggested that calcified cartilage provides an intermediate stiffness, reducing the mismatch of the stiffness modulus between hyaline cartilage and bone.[16,17] On the other hand, at the tissue level, when using nanoindentation, the calcified cartilage and underlying bone were found to have similar mechanical stiffness.[12,18,19] These studies have also measured mineralization and reported that the mineralization–modulus relation in calcified cartilage and subchondral bone are different, where more mineral is needed in calcified cartilage to achieve the same stiffness and hardness level as underlying bone.[12]

Osteoarthritis (OA) is a degenerative disease that targets most joint tissues. Osteochondral tissues have hierarchical structures that change over multiple length scales. In articular cartilage, early disease processes involve chondrocyte apoptosis/proliferation and surface fibrillation/edema, which develops to surface discontinuity accompanied by proteoglycan loss. In moderate OA, vertical fissures appear in the articular cartilage followed by cartilage matrix erosion with more evident proteoglycan loss and possibly some collagen formation.[20] Subchondral bone sclerosis is a known hallmark of OA. We have suggested that the thickening of bone structures is a synchronous process with cartilage degeneration during OA progression.[21]

The calcified cartilage undergoes structural modifications during OA. Perhaps the most evident of the changes is described as the tidemark multiplication,[22,23] which has been linked to the advancement of calcified cartilage toward the articular cartilage.[23-25] However, several studies have reported that the roughness of tidemark is also linked with OA severity.[26-28] The topmost tidemark defines the calcification front presenting tidemark multiplication, which increases the thickness of calcified cartilage. However, two processes could also make calcified cartilage thinner. First, a process similar to endochondral ossification, where deep calcified cartilage is replaced by bone,[29,30] increases the subchondral bone thickness, and thins the calcified cartilage.[31] Second, erosion continues on the mineralized surfaces once all cartilage has been removed with denudation with severe OA.[20] Considering all of the structure modifying processes it is logical that the thickest calcified cartilage has been observed with moderate OA.[21,32,33]

Microstructural changes in subchondral bone and calcified cartilage contribute to sclerosis (*stiffening*) of the structures beneath the articular cartilage. Furthermore, the mineralization level modulates the stiffness of subchondral tissues.[19] Mineral crystal thickness has been reported to increase with age in rabbit bone,[34] as well as with the tensile modulus and strength of the collagen–hydroxyapatite interfaces.[35] However, the nanostructural changes in bone and calcified cartilage that are associated with OA are inadequately understood. Therefore, we aimed to quantify the nanostructural organization (ie, mineral crystal thickness, degree of orientation, and predominant orientation) by employing state-of-the-art microfocus small-angle X-ray scattering (μSAXS) in calcified cartilage and subchondral bone, and to compare the nanostructural organization between end-stage knees of OA patients and healthy knees of deceased donors. We hypothesized that mineral crystals are thicker in calcified cartilage than subchondral bone and that the mineral crystal thickness increases in OA, in both calcified cartilage and subchondral bone.

Materials and Methods

Tissue sample preparation

The osteochondral samples of both OA patients and deceased donors have been sourced from the MENIX biobank, a local biobank at Skåne University Hospital, Region Skåne, Sweden (principal investigator: ME). The osteochondral samples from load-bearing areas of medial and lateral femoral condyles (Fig. 1*A*) were obtained from 15 patients (eight women, seven men) with end-stage medial compartment knee OA, who underwent total knee replacement (TKR) at Trelleborg Hospital, Sweden (descriptive data: Table S1). Obtained femoral condyles were frozen at −80°C within 2 hours of extraction and delivered on dry ice to the biobank for further storage at −80°C. During the TKR surgery, the surgeon's Outerbridge classification[36] of the knee joint cartilage was required to be a grade IV in the medial compartment and grade 0 or I in the lateral compartment for the patient to be classified to have medial compartment OA.

In addition, the osteochondral samples from load-bearing areas of medial and lateral femoral condyles were collected from 10 deceased human donors (five women, five men). No known diagnosis of knee OA or rheumatoid arthritis was allowed for the donors who were included in this study. The femoral condyles were obtained within 48 hours postmortem and frozen at −80°C within 2 hours of extraction. The age range of donors was greater than TKR patients (descriptive data: Table S1). The heights of patients and donors were similar in both sexes. The osteochondral sample set was divided into four groups that will henceforth be referred to as (i) $\text{Medial}^{\text{TKR}}$ ($n = 15$), (ii) $\text{Lateral}^{\text{TKR}}$ ($n = 15$), (iii) $\text{Medial}^{\text{Donor}}$ ($n = 10$), and (iv) $\text{Lateral}^{\text{Donor}}$ ($n = 10$). This study was approved by the regional ethical review board (Lund University; Dnr 2015/39 and Dnr 2016/865).

On the sample preparation day, the medial and lateral femoral condyles from both TKR and donor samples were thawed and further trimmed into a diameter of 5 mm with a trephine drill or a low-speed diamond saw, respectively. The samples were fixed in 4% saline-buffered formaldehyde for 7 days at 4°C and then in 70% ethanol for 24 hours. The sample processing continued with dehydration in ascending ethanol concentrations (80%, 95%, 100%, 100%), each step lasting for at least 6 hours. After dehydration, the samples were embedded in polymethylmethacrylate (PMMA). To deactivate the monomer, methyl methacrylate (MMA) was filtered through a column filled with aluminum oxide.

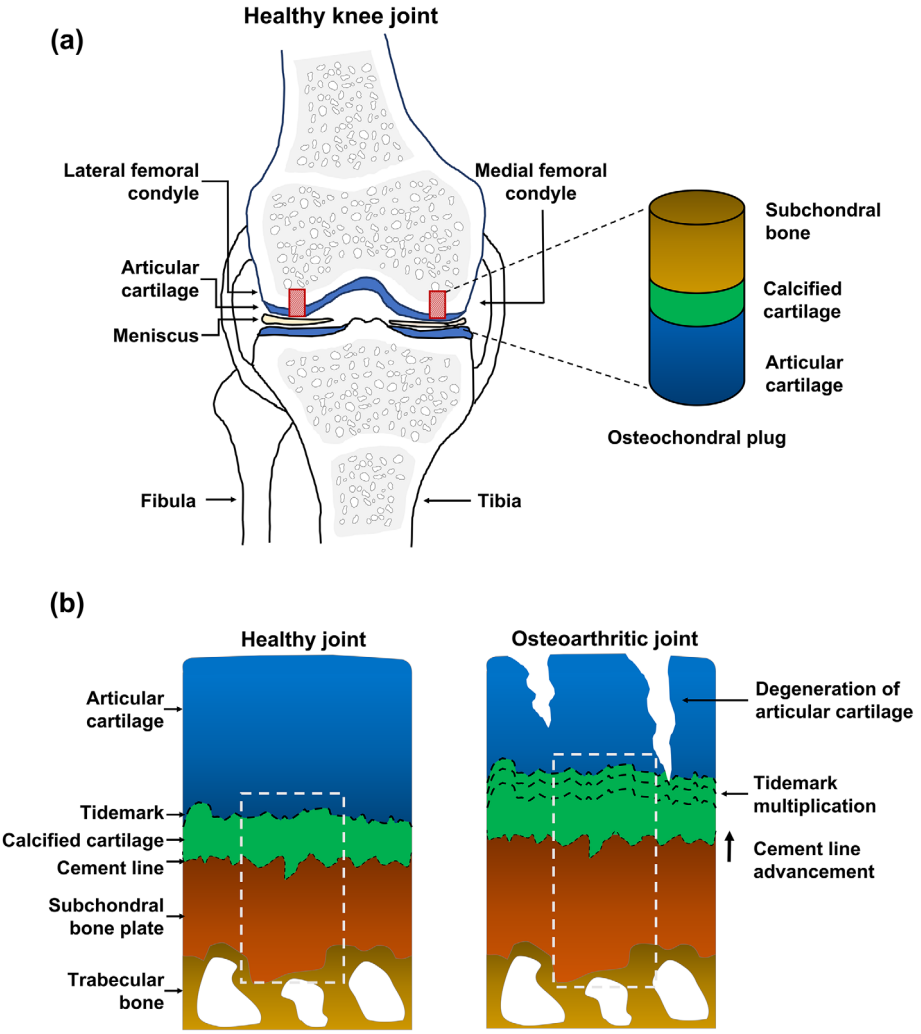

Fig. 1. Schematic representation of osteochondral sample collection and μSAXS measurement of healthy and osteoarthritic knee joints. (*A*) Osteochondral plugs were collected from both lateral and medial femoral condyles. (*B*) Schematic cross-sectional representation of samples taken from healthy and osteoarthritic knee joints. The white dotted line represents the 500 μm wide μSAXS measurement area extending from the deep articular cartilage to the subchondral bone (500–1000 μm).

The samples were infiltrated first with MMA in a solution containing deactivated MMA, 1.4 (vol%) nonylphenyl-polyethylene glycol acetate, and 5.5 μg/mL Benzoyl peroxide at 4°C for 24 hours, after which the solution was replaced with a fresh one. In the final step, the container with the previous solution was filled with an additional 5 μL/mL of N,N-Dimethyl-p-toluidine for plastification. The plastification was completed in the following 24 hours at 4°C.

Histological analyses

A histopathological evaluation of the osteochondral samples was performed according to the Osteoarthritis Research Society International (OARSI) grading system.[20] The histopathological evaluation solely focuses on changes of the articular cartilage from mild to advanced OA, and subchondral bone modifications are only accounted for in the final grades.[20] Because most of the histopathological evaluation accounts for only articular cartilage modifications, it can be considered as the golden standard for cartilage degeneration. Six histological sections (3-μm-thick) were cut from the PMMA blocks with a microtome (Leica Polycut S Microtome; Leica, Lucia, Germany) followed by Safranin-O or Goldner trichrome staining. The stained sections were used for the OARSI grading and counting the number of tidemarks, respectively. The number of tidemarks reflects the tidemark advancement, a process in which calcified cartilage extends into articular cartilage.[20] The OARSI grading was first conducted independently by two readers (MAJF, IH; interobserver reliability: intraclass correlation coefficient (ICC) 0.85 (95% confidence interval [CI], 0.69–0.93) for medial osteochondral samples and ICC 0.79 (95% CI, 0.58–0.90) for lateral osteochondral samples], and their consensus grade was given as a final grade for each sample.

SAXS

SAXS measurements were conducted at the state-of-the-art cSAXS (X12SA Coherent Small-Angle X-ray Scattering beamline at the Swiss Light Source; Paul Scherrer Institute, Villigen, Switzerland). From the PMMA blocks, 5-μm-thick osteochondral sections were

cut adjacent to the histological sections using a microtome (Leica Polycut S Microtome) and fixed on Kapton tape. Photon energy was set to 12.4 keV and the beam at the sample position was focused to 5 × 5 μm^2. SAXS patterns were recorded with a Pilatus 2 M detector[37] placed 7.1 m from the sample and using 30 ms exposure time per point. A 500-µm-wide area (Fig. 1*B*) extending from the tidemark to the bone marrow (500–1000 µm) was scanned with a 5-µm step size in a continuous line-scan mode.

Recorded scattering patterns were azimuthally integrated to obtain the intensity I as a function of scattering vector q, I(q) scattering curves.[38] The mineral crystal thickness at each point was evaluated from the I(q) scattering curves by using weighted iterative curve fittings at the q-range of 0.32–1.40 nm^{-1}.[39] In the fitted model, developed by Bünger and colleagues,[40] the dimensions of mineral crystal are assumed such that the scattering takes place from the mineral plates with finite thickness and infinite size in two other dimensions (length and width). The fitting and analysis of the mineral crystal thickness was identical as described by Turunen and colleagues[39] and the analysis method is based on what was described earlier by Bünger and colleagues.[40] In brief, the final expression of the total scattering intensity used of the fitted model is: $I(q) = P_{eff}(q) + B$; here, P_{eff} is the effective plate scattering, and B is the background term that is added to the fit.

The degree of orientation is an indicator of the number of aligned crystals in ratio to the illuminated sample volume and describes information about the mineral quality. The degree of orientation was obtained by fitting Gaussian curves to the two symmetrical peaks of the azimuthal dependence I(Ψ) and expressed as the ratio between the anisotropic scattering (area under the two Gaussian curves) and the total scattering within the illuminated sample region (area under the Gaussian curves with the constant background).[41] This ratio does not have a unit (arbitrary unit [a.u.]) and it is expressed as a value that varies between 0 and 1, where 0 represents a random mutual alignment and 1 represents a perfect alignment of the mineral crystals. Similarly, the predominant orientation of the crystals was estimated from the azimuthal dependence of SAXS signals. Because the positions (angles) of those two symmetrical peaks directly provides the predominant orientation of the mineral crystals rotated by 90 degrees,[42] the predominant orientation of the crystals was calculated by adding 90 degrees to the positions of Gaussian curves and expressed as a value between 0 degrees and 180 degrees.

Calcified cartilage and subchondral bone were identified by using unsupervised *K*-means clustering of the fitted I(q) curves. The cluster results were verified by comparing the cluster image to the histological images of the adjacent sections and cSAXS visualizations combining the predominant orientation and the asymmetric intensity at the q-range of 0.024–0.441 nm^{-1} (Figs. S1 and S2). Typically, eight clusters provided meaningful segmentation, but if the reference images indicated incorrect tissue identification, then the number of clusters was iteratively increased until accurate identification was achieved or a maximum number of 20 clusters was reached. All analysis steps of SAXS signals including the cluster analysis were carried out using in-house Matlab code (R2019a; MathWorks Inc., Natick, MA, USA) and the cSAXS Matlab package.[38]

Statistical analyses

For all statistical analyses, the tissue-specific mean values of SAXS parameters (ie, mineral crystal thickness and the degree of orientation) were derived from each sample. The between-group differences of SAXS parameters were estimated using linear mixed-effects models where the individual was included as a random effect. The patient status (ie, donor or TKR), the compartment (ie, medial or lateral), and their interactions were included in the model. Additionally, the models were adjusted for patient age and body mass index (BMI), they were included as continuous independent variables in the regression model. Due to the small sample size, Kenward and Roger's method was used for estimating the number of degrees of freedom. Moreover, similar linear mixed-effects models were used to estimate the differences in the SAXS parameters between the tissue types (ie, calcified cartilage and subchondral bone), as well as between two different layers of calcified cartilage. When calculating the difference between the tissue types, the patient status, compartment, tissue types, and their interactions were included as fixed effects, whereas the individual and compartment (compartments nested in individuals) were set as random effects. In the analysis of calcified cartilage layers, the patient status was not included since only three donor samples had multiple tidemarks. Thus, the compartment, layer, and their interaction were included as fixed effects in the analysis of calcified cartilage layers. The estimates

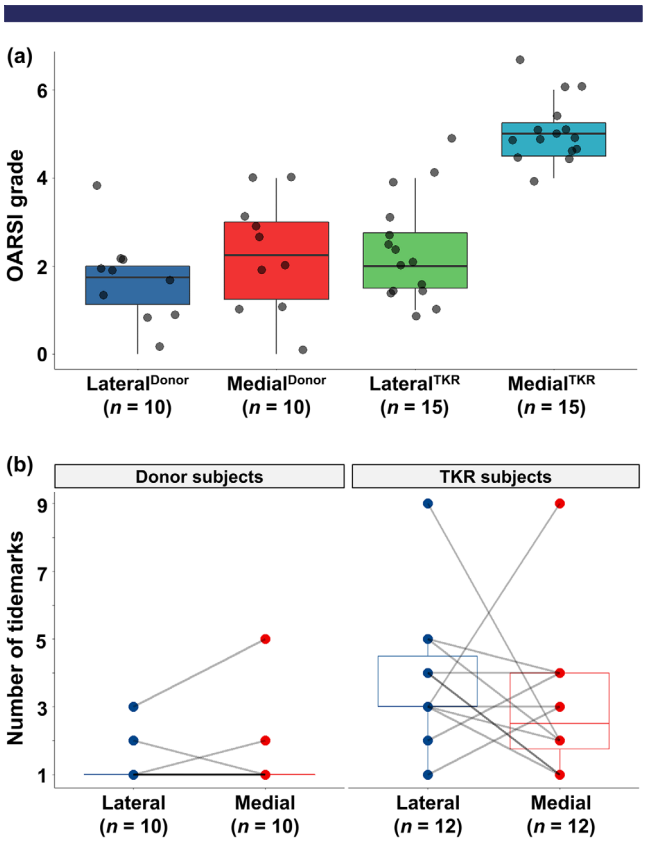

Fig. 2. Histopathological assessment of the osteochondral samples. (*A*) Box plot with jitter showing the OARSI grades (with subgrades) in the lateral and medial condyles of cadaveric donors and total knee replacement (TKR) patients. Each grade represents the following key feature. Grade 0: Fully intact cartilage; grade 1: Intact surface with cellular changes and/or edema; grade 2: Surface discontinuity; grade 3: Vertical fissures; grade 4: Cartilage erosion; grade 5: Denudation (articular cartilage matrix loss to calcified cartilage); and grade 6: Deformation. (*B*) Box plot with a pairwise comparison showing the number of tidemarks, which were counted from the histopathological images. There was complete erosion of calcified cartilage in three samples from the Medial^{TKR} group and these patients were excluded from the pairwise comparison.

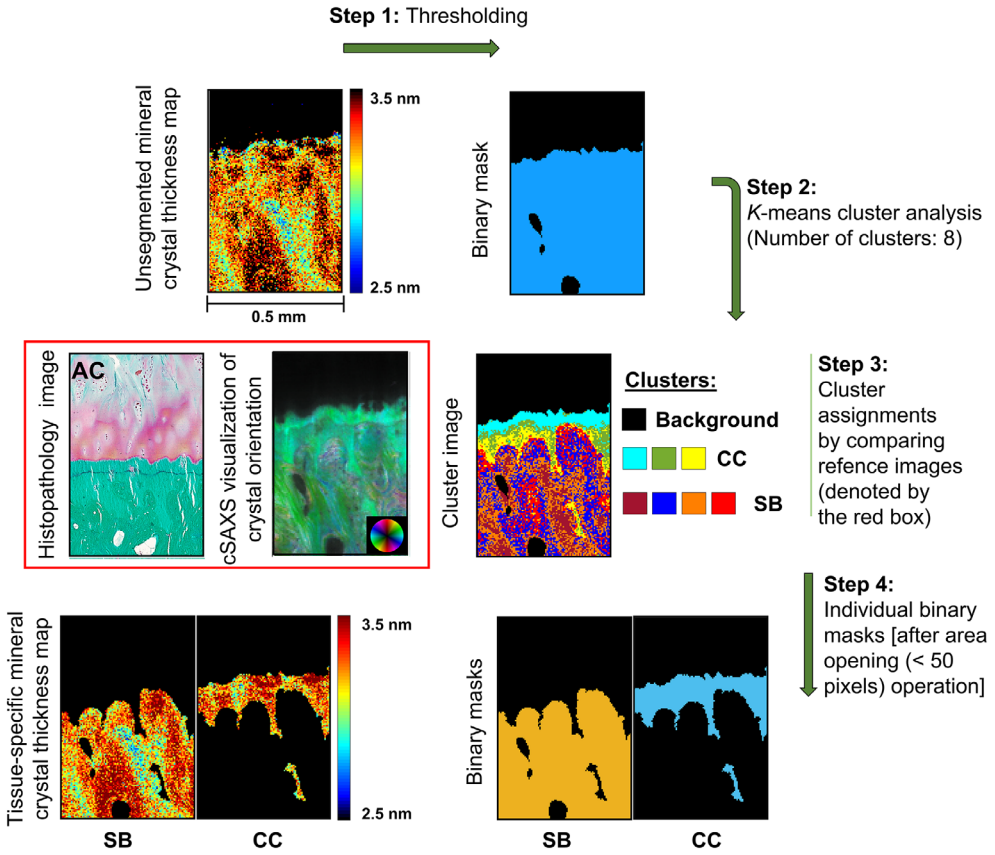

Fig. 3. Tissue segmentation from 2D μSAXS images. Step 1: The mineral crystal thickness maps were binarized using an absolute threshold on scattering intensity. Step 2: *K*-means cluster analysis of the I(*q*) scattering curves. Step 3: Eight clusters were found to be optimal for most of the samples when comparing the cluster images to the cSAXS visualizations of crystal orientation and asymmetric intensity. The cluster assignments were further confirmed by comparing the cluster images to the histopathological images of adjacent sections. Step 4: Final tissue-specific binary masks for CC and SB were generated after de-speckling. CC = calcified cartilage; SB = subchondral bone.

Table 1. SAXS Parameters From the Superior and Inferior Layers of Calcified Cartilage in Samples With Multiple Tidemarks (15 Osteochondral Samples From the Lateral Compartment and 8 From the Medial Compartment)

	Mineral crystal thickness (nm)			
Compartment location	Superior CC	Inferior CC	Difference (95% CI)	*p*
Lateral ($n = 15$)	3.64 (0.28)	3.27 (0.16)	0.36 (0.24–0.49)	<0.001
Medial ($n = 8$)	3.36 (0.26)	3.13 (0.09)	0.23 (0.06–0.40)	0.01
	Degree of orientation (a.u.)			
Lateral	0.65 (0.03)	0.63 (0.03)	0.02 (0.02–0.03)	<0.001
Medial	0.64 (0.02)	0.63 (0.03)	0.01 (0.00–0.02)	0.06

Results are displayed as means (standard deviations) of the SAXS parameters from the superior and inferior calcified cartilage layers along with the difference (with 95% confidence interval and *p* value) between them, in both medial and lateral compartments, respectively.
CC = calcified cartilage.

are presented with a 95% CI. Because the predominant orientation of mineral crystal is heavily dependent on bone structures being included in the measurement region, no statistical analysis of the predominant orientation information was performed; rather only their distribution across the calcified cartilage and subchondral bone were presented. All statistical analyses were performed using Stata version 17 software (STATA Corp., College Station, TX, USA).

Results

Histopathological severity of OA and tidemark multiplication

In the cadaveric donors, we observed relatively healthy cartilage with intact surface or focal fibrillation through the superficial zone (Fig. 2*A*). Five donor samples showed features of mild OA; vertical fissures and even cartilage matrix losses were present. All samples

Table 2. SAXS Parameters From the Calcified Cartilage and Subchondral Bone Along With the Difference (With 95% Confidence Interval and *p* Value) Between them, in Both Medial and Lateral Compartments of Cadaveric Donors (Donor) and TKR Patients

Group	Mineral crystal thickness (nm)		Difference (95% CI)	*p*
	Calcified cartilage	Subchondral bone		
Lateral^{Donor}	3.15 (0.17)	3.01 (0.21)	0.14 (0.04–0.23)	0.01
Medial^{Donor}	3.19 (0.19)	2.97 (0.16)	0.19 (0.10–0.29)	<0.001
Lateral^{TKR}	3.41 (0.16)	3.19 (0.19)	0.26 (0.19–0.34)	<0.001
Medial^{TKR}	3.25 (0.10)	3.03 (0.12)	0.22 (0.14–0.31)	<0.001
	Degree of orientation (a.u.)			
Lateral^{Donor}	0.64 (0.03)	0.61 (0.02)	0.03 (0.01–0.04)	<0.01
Medial^{Donor}	0.65 (0.02)	0.60 (0.01)	0.04 (0.03–0.06)	<0.001
Lateral^{TKR}	0.63 (0.03)	0.60 (0.01)	0.04 (0.02–0.05)	<0.001
Medial^{TKR}	0.62 (0.05)	0.59 (0.02)	0.03 (0.02–0.05)	<0.001

Values are means (standard deviations).
TKR = total knee replacement.

from the Medial^{TKR} group had a loss of cartilage matrix and in some cases, there were also erosions of calcified cartilage. The OARSI grade distribution in the lateral compartment of TKR patients resembled the grade distribution in the medial side of the cadaveric donors (Fig. 2*A*). Moreover, we observed higher tidemark counts in TKR patients compared to the donors. However, we could not identify any clear pattern for tidemark multiplication between the medial and lateral compartments (Fig. 2*B*).

SAXS analysis of mineral crystals in the osteochondral junction

Calcified cartilage and subchondral bone were segmented based on the fitted I(*q*) scattering curves by utilizing unsupervised *K*-means clustering (Fig. 3). This allowed for spatially resolving the SAXS parameters (ie, mineral crystal thickness, the degree of orientation, and predominant orientation) separately for calcified cartilage and subchondral bone (Figs. S3–S8). Furthermore, we observed that the uppermost cluster(s) in calcified cartilage was co-localized with a layer between two topmost tidemarks in the calcified cartilage (Fig. S9). Hence, based on the cluster analysis, we further segmented the calcified cartilage into two layers (ie, superior and inferior). Although the superior calcified cartilage layer is separated by the two topmost tidemarks, the inferior layer is the rest of the calcified cartilage below the second-to-top tidemark. Interestingly, the mineral crystals in the superior layer appear to be thicker and more mutually aligned compared to the inferior layer of the calcified cartilage (Table 1, Fig. 4).

Mineral crystal thicknesses and degree of orientation in cadaveric donors and total knee replacement patients

Mineral crystal thicknesses in the subchondral bone were around 3.0 nm in Medial^{TKR}, Medial^{Donor}, and Lateral^{Donor} groups; whereas, the Lateral^{TKR} group had 3.19-nm-thick crystals on average (Table 2). In all groups, the mineral crystal thicknesses in calcified cartilage were higher compared to those in the subchondral bone (Table 2). Moreover, the degree of orientation in calcified cartilage was higher in all groups (4.8% in Medial^{TKR}, 6.2% in Medial^{Donor}, 6.3% in Lateral^{TKR}, and 4.7% in Lateral^{Donor} group) compared to the adjacent bone (Table 2). Furthermore, the distributions of the predominant orientation in the calcified cartilage show that the long axis (c-axis) of mineral crystals was

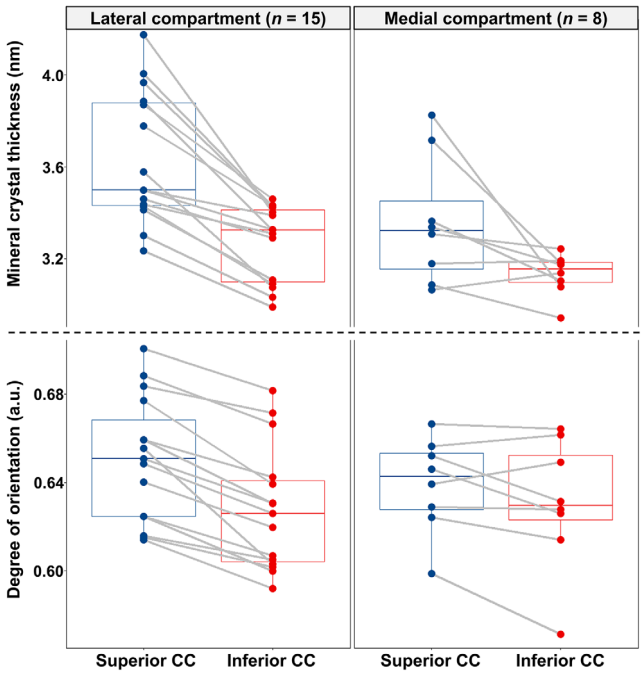

Fig. 4. SAXS parameters in the two layers of CC of the samples with tidemark multiplication. Box plots showing the pairwise comparison of the mineral crystal thickness and degree of orientation between the superior and inferior layers of calcified cartilage in the osteochondral samples with multiple tidemarks, from both lateral (15 samples) and medial (8 samples) compartments, respectively. CC = calcified cartilage.

almost aligned with collagen fibrils (Figs. S1, S2, S7, and S8). Similarly, the predominant orientation of mineral crystals in the subchondral bone followed the alignment of collagen fibrils, even around the osteons and trabeculae (Figs. S1, S2, S7, and S8).

In the subchondral bone, the difference between Lateral^{TKR} and Medial^{TKR} was 0.17 nm (95% CI, 0.03–0.31), and between Lateral^{donor} and Lateral^{TKR} 0.17 nm (95% CI, 0.08–0.26). However, this difference diminishes after adjusting for age (Fig. 5). The mineral crystal thickness in calcified cartilage was the highest

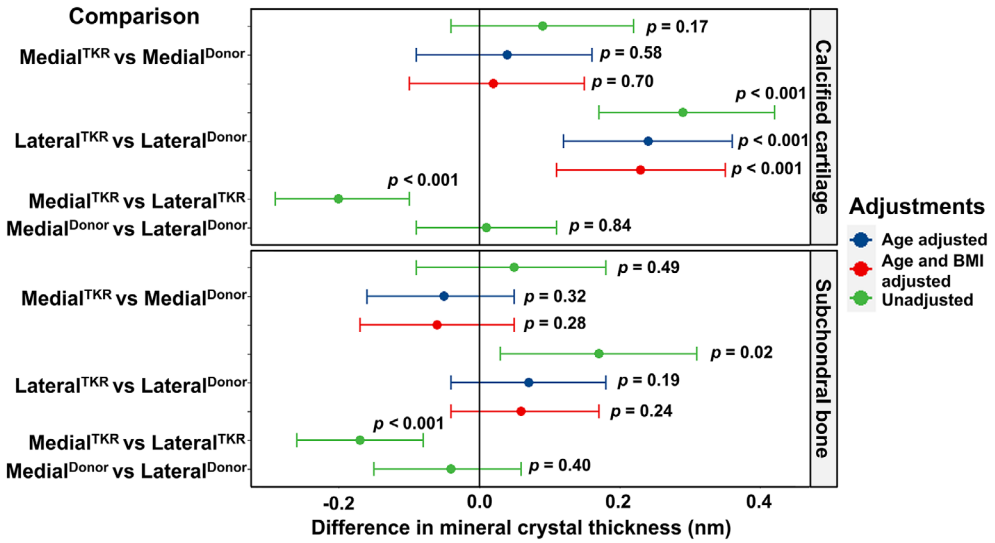

Fig. 5. Compartment-specific comparison of the mineral crystal thickness between cadaveric donors (donor) and TKR patients. Differences in mineral crystal thickness are displayed with a 95% confidence interval and *p* value in the calcified cartilage and the subchondral bone, respectively. The model was adjusted for age, and then for age and BMI. The comparison between medial and lateral compartments from the same knee is adjusted for all individual- and knee-level confounding through the design and use of a mixed-effects model. TKR = total knee replacement.

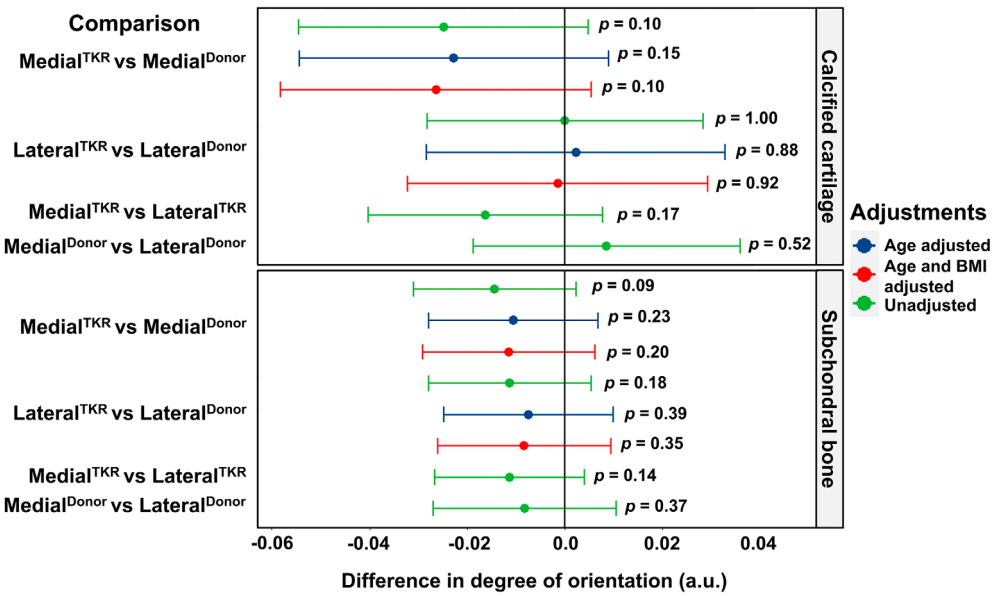

Fig. 6. Compartment-specific comparison of the degree of orientation of mineral crystals in the calcified cartilage and the subchondral bone between cadaveric donors (donor) and TKR patients. Differences in the degree of orientation are displayed with a 95% confidence interval and *p* value. The mixed-effects model was adjusted for age, and then for age and BMI. TKR = total knee replacement.

in the Lateral^{TKR} group and the difference after adjusting for age and BMI remained at 0.2 nm (95% CI, 0.10–0.29) and 0.23 nm (95% CI, 0.11–0.35) when compared to Medial^{TKR} or Lateral^{donor}, respectively (Fig. 5).

Finally, in calcified cartilage, we found that the Medial^{TKR} group tended to have a −0.03 (95% CI, −0.06 to 0.01) smaller degree of orientation (a.u.) compared to the Medial^{Donor} group (Fig. 6). However, in the Lateral^{TKR} and Lateral^{Donor} groups, the degree of orientation in calcified cartilage was similar. Furthermore, the degree of orientation in subchondral bone also remained unchanged in TKR patients in both medial and lateral compartments compared to donors (Fig. 6).

Discussion

In this study, we spatially mapped the mineral crystal thickness, degree of orientation, and predominant orientation of mineral crystals across the osteochondral junction in healthy and osteoarthritic human knees using state-of-the-art μSAXS. There were three major findings in our study: (i) we found that the mineral crystals are thicker and more aligned in calcified cartilage than in subchondral bone; (ii) we identified that the mineral crystal thickness and the degree of orientation are higher in the superior layer than in the inferior layer of calcified cartilage. This superior layer of the calcified cartilage is associated with pathological tidemark multiplication; and (iii) we observed the thickest mineral crystals in both osteochondral tissues in the lateral compartment of TKR patients with medial compartment OA.

The orientation and morphology of the mineral crystals have major implications for mechanical behavior by controlling anisotropy and hardness.[43,44] Modern evidence using a combination of three-dimensional (3D) electron tomography and two-dimensional (2D) electron microscopy suggests a fractal-like hierarchical bone architecture, where needle-shaped mineral crystals merge laterally to form platelets that organize into stacks of roughly parallel platelets (thickness 5 nm) bridging multiple collagen units.[45] The thickness of the mineral crystal is commonly assumed to be regulated by the structure of the organic matrix[46] and by noncollagenous proteins.[47] Given the fact that the calcified cartilage and subchondral bone have different organic matrices, it is crucial to study the nanostructural organization of these tissues, individually in health and disease. However, owing to limitations in the spatial resolution or contrast of current nondestructive techniques, possible OA-related changes in the nanostructural organization of these osteochondral tissues have not been studied until now.

Zizak and colleagues[48] have reported that the calcified cartilage possesses a similar mineral crystal size, shape, and orientation to that of underlying bone. In contrast, we report thicker mineral crystals in the calcified cartilage compared to the subchondral bone. This finding is aligned with our previous investigation of the human osteochondral junction by using Raman microspectroscopy, where a higher degree of mineralization and more stoichiometric perfect crystal lattice was found in the calcified cartilage compared to the cortical subchondral bone.[15] Accordingly, we propose that the thicker mineral crystal might be related to the fewer nonstoichiometric substitutions of carbonate for phosphate ions in the crystal lattice of calcified cartilage compared to the bone. The substitutions of carbonate in the apatite crystal lattice are reported to decrease mineral crystallinity, as well as cause contraction of the a-axis and expansion of the c-axis dimensions of the unit cell.[49,50] The orientation of the mineral crystals is aligned with the collagen fiber orientation, in both calcified cartilage and subchondral bone. However, on average, the degree of orientation of calcified cartilage is higher than in subchondral bone. This might be due to the highly aligned collagen matrix in the calcified cartilage, whereas in subchondral bone collagen fibrils follow lamellar structure.

It has been proposed that the mineral crystal thickness and alignment in osteochondral tissues might be governed by organic matrix and noncollagenous proteins.[48] Indeed, one of the possible explanations for differences in mineral crystal growth could be the differences in the organic matrices of calcified cartilage and subchondral bone. The organic matrix of cartilage has a higher amount of extrafibrillar space filled with water than that of bone. Water makes up about 10% to 20% of the volume of cortical bone and can drop to as low as 5% with increasing age,[51] whereas water composes about 60% to 85% of normal adult cartilage.[52] This availability of extrafibrillar space might allow the growth of thicker crystals in the calcified cartilage than in the adjacent bone. In addition, pyrophosphate is a potent inhibitor of mineral formation, which inhibits crystal growth.[53,54] Important regulators for the pyrophosphate in calcified cartilage and subchondral bone include tissue nonspecific alkaline phosphatase (TNAP), plasma cell membrane glycoprotein-1 (PC-1/NPP1), and the Ankylosis protein (*Ank*).[53,54] TNAP hydrolyzes pyrophosphate and is an important inducer of mineralization.[55] On the other hand, the concentration of the extracellular pyrophosphate increases due to the accelerated activities of NPP1 and *Ank*.[53] There is further evidence that NPP1 expression would decline with OA.[56]

Second, we identified thicker and more aligned mineral crystals in the superior layer of calcified cartilage. Fawns and Landell,[57] in 1953, were among the first to describe "tidemark" as the most recent calcified border of calcified cartilage, using histological staining. The presence of two or more tidemarks (tidemark multiplication) is a sign of advancement of calcified cartilage into articular cartilage, which is not exclusive to osteoarthritic joints; this may also occur with aging,[58] change in loading states,[59] and exercise.[60] The noncontinuous but periodic process of upward mineralization of articular cartilage, indicated by tidemark multiplication, was demonstrated in the femoral heads of mature rabbits already in 1971 by Lemperg[61] and in osteoarthritic human joints by Green and colleagues.[62] There appears to be a similar endochondral ossification process in the calcified cartilage that occurs in long bones during growth.[63,64] In this ossification process, chondrocytes near the tidemark are shown to have a hypertrophic phenotype, express type X collagen,[65] and become mineralized. Poorly crystalline calcium inorganic orthophosphate nanocrystals are deposited around the chondrocytes in the organic matrix of the cartilage promoting the advancement of calcified cartilage.[66] It is traditionally accepted that the endochondral ossification process for skeletal development and fracture repair involves the apoptosis of those hypertrophic chondrocytes followed by the vascular invasion of mesenchymal stem cells. A similar process most likely occurs in calcified cartilage, because vascular invasion and pore/channel formation through calcified cartilage have been observed in OA. Furthermore, chondrocyte-to-osteoblast transdifferentiation has been reported in calcified cartilage and could promote ossification along with the canonical pathway of endochondral ossification.[67-69] However, the role of chondrocyte transdifferentiation in OA-related bone deposition should be further investigated. Previous studies have reported a higher level of mineralization near tidemark than in the region of calcified cartilage near the bone with quantitative backscattered electron imaging.[12,18] In the present study, there were more tidemarks in TKR patients compared to donors (Fig. 2). Using cluster analysis, in the samples with multiple tidemarks, we related the uppermost cluster to the layer of calcified cartilage separated by two topmost tidemarks. We propose that this layer (ie, the superior layer of the calcified cartilage) is indicative of the most recently mineralized layer of calcified cartilage due to ossification. Remarkably, we observed the thickest mineral crystal in this superior calcified cartilage layer (Fig. 4). This could not be observed in our previous Raman study[15] and to our knowledge, this has not been reported before in the literature. This may indicate that during the tidemark advancement the mineral crystals have greater thickness after deposition, and they restructure to

thinner mineral plates with maturation. Eventually, the calcified cartilage substance is removed by osteoclasts (carried by capillaries) and then replaced by bone substance synthesized by osteoblasts during new bone formation.[66]

Finally, the present study allows a detailed spatial comparison of nanostructural organization and OA severity assessed with histopathology. We compared both lateral and medial compartments of the femoral osteochondral junction from TKR patients with end-stage medial compartment knee OA and deceased donors without known OA. We found that the lateral compartment of the TKR patients has the thickest mineral crystals in both subchondral bone and calcified cartilage (Fig. 5). Importantly, these changes occur in the osteochondral mineralized tissues of the lateral compartment, whereas the greatest cartilage degeneration (as indicated by histopathological assessment) occurs in the medial compartment. Thus, the difference between TKR patients and donors found in mineral crystal thickness in the lateral compartment's calcified cartilage indicates that mineralization is an independent process compared to cartilage degeneration, at least in our particular sample set. This is further supported by the fact that mineral crystal thickness is higher in calcified cartilage in the $Lateral^{TKR}$ compared to $Lateral^{Donor}$ even after adjusting for age and BMI. In subchondral bone, age adjustment reduces the difference in group-wise comparison.

Because the TKR patients had end-stage knee OA on the medial compartment, we expected to find changes in mineral crystal thickness in this compartment. Surprisingly, we observed increased mineral crystal thickness in the lateral compartment, with apparently "healthy" cartilage. In individuals with a healthy knee joint, during the gait cycle in normal walking, the load distribution is not equal between the medial and lateral tibiofemoral compartments and the medial compartment exhibits higher loads.[70,71] The medial shift of the load-bearing axis due to varus alignment further increases loading across the medial compartment.[71,72] It has been reported that the absolute load (normalized to body weight) is increased in OA and due to mediolateral loading distribution, a relatively high proportion of the load is subjected over the medial compartment.[73] In the same study, one-half of the subjects with medial compartment knee OA demonstrated unloading of the lateral compartment in mid to late stance.[73] An increase in joint loading and cartilage stress are commonly considered to be related to bone architecture alteration and cartilage degeneration, respectively.[64] Previous studies showed that abnormal loads may start a remodeling response in bone[74,75] and induce changes in composition and mechanical properties in cartilage,[76] respectively. Thus, the increased mineral crystal thickness in the lateral compartment could be related to biomechanics. This is further supported by a study from O'Connor who reported increased mineral apposition and tidemark advancement after experimental unweighting of hind limbs in rats.[59]

There are a few limitations in the current study. First, we do not have a perfect overlap in the subject age between donor and TKR groups; the age of the donor group ranges from 18 to 77 years whereas the TKR patients range from 50 to 79 years. This needs to be considered carefully during the interpretation of findings, despite the fact we have reported both age and BMI-adjusted findings. Second, we have used the same curve fitting model to determine the mineral crystal thickness for both subchondral bone and calcified cartilage. Hence, the adjustable parameters like the width of the crystallite thickness distribution, the random phase approximation value, and the effective structure factor were assumed to be the same for both tissues.[39,40] However, even with these limitations, this study represents a state-of-the-art application of μSAXS in investigating the nanostructural organization across the osteochondral junction using a full range of histopathological OA severities. The classification of the scattering curves of the calcified cartilage and the subchondral bone using an unsupervised clustering approach further extends the strength of the study.

In summary, we observed increased mineral crystal thickness in calcified cartilage and subchondral bone of the unloaded compartment in the patients with the medial compartment knee OA. These results indicate that the mineralization of osteochondral tissues might be an independent process from cartilage erosion, and it can be driven by a lack of local mechanical loading. Our findings indicate that loading is an important factor for biomineralization of calcified cartilage during OA development, and could be exploited when developing tissue engineering strategies for the osteochondral interface.

Acknowledgments

Author MAJF received funding for this work from the Finnish Cultural Foundation (North Ostrobothnia Regional Fund No. 60172246). Author SDG was supported by funding from the European Union's Horizon 2020 research and innovation program under the Marie Skłodowska-Curie grant agreement no. 713645. Author IH was supported by funding from the Finnish Foundation for Technology Promotion. Author HI acknowledge funding from the Swedish Research Council (2019-00953) under the frame of ERA PerMed. Author SS acknowledges grants from the Academy of Finland (Grants No. 268378, and 303786) and grants from the European Research Council under the European Union's Seventh Framework Program (FP/2007–2013; ERC Grant Agreement No. 336267), during conduction of this study. Author ME acknowledges grant support from the Swedish Research Council, The Swedish Rheumatology Association, Österlund Foundation, and the Governmental funding of clinical research within the national health services (ALF); other authors have no disclosures in relation to this manuscript. We acknowledge the Paul Scherrer Institut, Villigen PSI, Switzerland for the provision of synchrotron radiation beamtime at the cSAXS beamline X12SA of the SLS. Moreover, we thank Ms. Tarja Huhta for preparing the histological sections.

Author Contributions

Mikko A.J. Finnilä: Conceptualization; investigation; methodology; software; writing – original draft; writing – review and editing. **Shuvashis Das Gupta:** Investigation; software; visualization; writing – original draft; writing – review and editing. **Mikael J. Turunen:** Conceptualization; investigation; software; writing – review and editing. **Iida Hellberg:** Investigation; writing – review and editing. **Aleksandra Turkiewicz:** Investigation; software; writing – review and editing. **Viviane Lutz-Bueno:** Investigation; writing – review and editing. **Elin Folkesson:** Methodology; writing – review and editing. **Mirko Holler:** Investigation; writing – review and editing. **Neserin Ali:** Methodology; writing – review and editing. **Velocity Hughes:** Methodology; writing – review and editing. **Hanna Isaksson:** Investigation; writing – review and editing. **Jon Tjörnstrand:** Methodology; writing – review and editing. **Patrik Önnerfjord:** Methodology; writing – review and editing. **Manuel Guizar-Sicairos:** Investigation; writing – review and editing. **Simo Saarakkala:**

Conceptualization; supervision; writing – review and editing. **Martin Englund:** Conceptualization; supervision; writing – review and editing.

Peer Review

The peer review history for this article is available at https://publons.com/publon/10.1002/jbmr.4642.

Data Availability Statement

Data used for this study can be made available by submitting on reasonable request to the corresponding author.

References

1. Lai WM, Hou JS, Mow VC. A triphasic theory for the swelling and deformation behaviors of articular cartilage. J Biomech Eng. 1991; 113(3):245-258.
2. Canal Guterl C, Hung CT, Ateshian GA. Electrostatic and non-electrostatic contributions of proteoglycans to the compressive equilibrium modulus of bovine articular cartilage. J Biomech. 2010;43(7): 1343-1350. https://doi.org/10.1016/j.jbiomech.2010.01.021.
3. Benninghoff A. Shape and composition of articular cartilage with regard to its function. II. Composition of articular cartilage with regard to its function [Form und Bau der Gelenkknorpel in ihren Beziehungen zur Funktion]. Zeitschrift fur Zellforschung und Mikroskopische Anatomie. 1925;2:783-862.
4. Thambyah A, Broom N. Micro-anatomical response of cartilage-on-bone to compression: mechanisms of deformation within and beyond the directly loaded matrix. J Anat. 2006;209(5):611-622.
5. Sophia Fox AJ, Bedi A, Rodeo SA. The basic science of articular cartilage: structure, composition, and function. Sports Health. 2009;1(6): 461-468.
6. Clark JM, Huber JD. The structure of the human subchondral plate. J Bone Joint Surg Br. 1990;72:866-873.
7. Burr DB. The contribution of the organic matrix to bone's material properties. Bone. 2002;31(1):8-11.
8. Wang X, Bank RA, TeKoppele JM, Mauli AC. The role of collagen in determining bone mechanical properties. J Orthop Res. 2001;19(6): 1021-1026.
9. Radin EL, Martin RB, Burr DB, Caterson B, Boyd RD, Goodwin C. Effects of mechanical loading on the tissues of the rabbit knee. J Orthop Res. 1984;2(3):221-234.
10. Karsdal MA, Michaelis M, Ladel C, et al. Disease-modifying treatments for osteoarthritis (DMOADs) of the knee and hip: lessons learned from failures and opportunities for the future. Osteoarthritis Cartilage. 2016;24(12):2013-2021. https://doi.org/10.1016/j.joca.2016.07.017.
11. Broom ND, Poole CA. A functional-morphological study of the tidemark region of articular cartilage maintained in a non-viable physiological condition. J Anat. 1982;135(Pt 1):65-82.
12. Gupta HS, Schratter S, Tesch W, et al. Two different correlations between nanoindentation modulus and mineral content in the bone-cartilage interface. J Struct Biol. 2005;149(2):138-148.
13. Roberts S. Collagen of the calcified layer of human articular cartilage. Experientia. 1985;41(9):1138-1139.
14. Fratzl P, Groschner M, Vogl G, et al. Mineral crystals in calcified tissues: a comparative study by SAXS. J Bone Miner Res. 1992;7(3):329-334.
15. Das Gupta S, Finnilä MAJ, Karhula SS, et al. Raman microspectroscopic analysis of the tissue-specific composition of the human osteochondral junction in osteoarthritis: a pilot study. Acta Biomater. 2020;106:145-155.
16. Mente PL, Lewis JL. Elastic modulus of calcified cartilage is an order of magnitude less than that of subchondral bone. J Orthop Res. 1994; 12(5):637-647. https://doi.org/10.1002/jor.1100120506.
17. Hargrave-Thomas E, van Sloun F, Dickinson M, Broom N, Thambyah A. Multi-scalar mechanical testing of the calcified cartilage and subchondral bone comparing healthy vs early degenerative states. Osteoarthritis Cartilage. 2015;23(10):1755-1762. https://doi.org/10.1016/j.joca.2015.05.012.
18. Ferguson VL, Bushby AJ, Firth EC, Howell PGT, Boyde A. Exercise does not affect stiffness and mineralisation of third metacarpal condylar subarticular calcified tissues in 2 year old thoroughbred racehorses. Eur Cells Mater. 2008;17(16):40-46.
19. Ferguson V, Bushby AJ, Boyde A. Nanomechanical properties and mineral concentration in articular calcified cartilage and subchondral bone. J Anat. 2003;203(2):191-202. https://doi.org/10.1046/j.1469-7580.2003.00193.x.
20. Pritzker KPH, Gay S, Jimenez SA, et al. Osteoarthritis cartilage histopathology: grading and staging. Osteoarthritis Cartilage. 2006;14(1): 13-29.
21. Finnilä MAJ, Thevenot J, Aho O-M, et al. Association between subchondral bone structure and osteoarthritis histopathological grade. J Orthop Res. 2017;35(4):785-792. https://doi.org/10.1002/jor.23312.
22. Allibone R, Meachim G. Topographical cartilage upper femoral. J Anat. 1984;139:341-352.
23. Goldring SR. Alterations in periarticular bone and cross talk between subchondral bone and articular cartilage in osteoarthritis. Ther Adv Musculoskelet Dis. 2012;4(4):249-258.
24. Thambyah A, Broom N. On new bone formation in the pre-osteoarthritic joint. Osteoarthritis Cartilage. 2009;17(4):456-463. https://doi.org/10.1016/j.joca.2008.09.005.
25. Goldring SR, Goldring MB. Changes in the osteochondral unit during osteoarthritis: structure, function and cartilage bone crosstalk. Nat Rev Rheumatol. 2016;12(11):632-644. https://doi.org/10.1038/nrrheum.2016.148.
26. Kauppinen S, Karhula SS, Thevenot J, et al. 3D morphometric analysis of calcified cartilage properties using micro-computed tomography. Osteoarthritis Cartilage. 2019;27(1):172-180.
27. Deng B, Wang F, Yin L, et al. Quantitative study on morphology of calcified cartilage zone in OARSI 0∼4 cartilage from osteoarthritic knees. Curr Res Transl Med. 2016;64(3):149-154.
28. Schultz M, Molligan J, Schon L, Zhang Z. Pathology of the calcified zone of articular cartilage in post-traumatic osteoarthritis in rat knees. PLoS One. 2015;10(3):1-12.
29. van der Kraan PM, van den Berg WB. Osteophytes: relevance and biology. Osteoarthritis Cartilage. 2007;15(3):237-244.
30. Van der Kraan PM, Van den Berg WB. Chondrocyte hypertrophy and osteoarthritis: role in initiation and progression of cartilage degeneration? Osteoarthritis Cartilage. 2012;20(3):223-232. https://doi.org/10.1016/j.joca.2011.12.003.
31. Florea C, Malo MKH, Rautiainen J, et al. Alterations in subchondral bone plate, trabecular bone and articular cartilage properties of rabbit femoral condyles at 4 weeks after anterior cruciate ligament transection. Osteoarthritis Cartilage. 2015;23(3):414-422.
32. Aho OM, Finnilä M, Thevenot J, Saarakkala S, Lehenkari P. Subchondral bone histology and grading in osteoarthritis. PLoS One. 2017; 12(3):1-16.
33. Burr DB, Gallant MA. Bone remodelling in osteoarthritis. Nat Rev Rheumatol. 2012;8(11):665-673. https://doi.org/10.1038/nrrheum.2012.130.
34. Törnquist E, Isaksson H, Turunen MJ. Mineralization of cortical bone during maturation and growth in rabbits. J Bone Miner Metab. 2020;38(3):289-298. https://doi.org/10.1007/s00774-019-01068-y.
35. Qin Z, Gautieri A, Nair AK, Inbar H, Buehler MJ. Thickness of hydroxyapatite nanocrystal controls mechanical properties of the collagen-hydroxyapatite interface. Langmuir. 2012;28(4):1982-1992.
36. Outerbridge RE. The etiology of chondromalacia patellae. J Bone Joint Surg Br. 1961;43(C):752-757.
37. Henrich B, Bergamaschi A, Broennimann C, et al. PILATUS: a single photon counting pixel detector for X-ray applications. Nucl Instrum Methods Phys Res A. 2009;607(1):247-249.

38. Bunk O, Bech M, Jensen TH, et al. Multimodal x-ray scatter imaging. New J Phys. 2009;11(12):123016. https://doi.org/10.1088/1367-2630/11/12/123016.
39. Turunen MJ, Kaspersen JD, Olsson U, et al. Bone mineral crystal size and organization vary across mature rat bone cortex. J Struct Biol. 2016;195(3):337-344.
40. Bünger MH, Oxlund H, Hansen TK, et al. Strontium and bone nanostructure in normal and ovariectomized rats investigated by scanning small-angle X-ray scattering. Calcif Tissue Int. 2010;86(4):294-306.
41. Turunen MJ, Lages S, Labrador A, et al. Evaluation of composition and mineral structure of callus tissue in rat femoral fracture. J Biomed Opt. 2014;19(2):025003.
42. Rinnerthaler S, Roschger P, Jakob HF, Nader A, Klaushofer K, Fratzl P. Scanning small angle X-ray scattering analysis of human bone sections. Calcif Tissue Int. 1999;64(5):422-429.
43. Ruppel ME, Miller LM, Burr DB. The effect of the microscopic and nanoscale structure on bone fragility. Osteoporos Int. 2008;19(9):1251-1265.
44. Sabet FA, Najafi AR, Hamed E, Jasiuk I. Modelling of bone fracture and strength at different length scales: a review. Interface Focus. 2016;6(1):20-30.
45. Reznikov N, Bilton M, Lari L, Stevens MM, Kröger R. Fractal-like hierarchical organization of bone begins at the nanoscale. Science. 2018;360(6388):eaao2189.
46. Fratzl P, Fratzl-Zelman N, Klaushofer K, Vogl G, Koller K. Nucleation and growth of mineral crystals in bone studied by small-angle X-ray scattering. Calcif Tissue Int. 1991;48(6):407-413.
47. Hunter GK, Hauschka PV, Poole AR, Rosenberg LC, Goldberg HA. Nucleation and inhibition of hydroxyapatite formation by mineralized tissue proteins. Biochem J. 1996;317(1):59-64.
48. Zizak I, Roschger P, Paris O, et al. Characteristics of mineral particles in the human bone/cartilage interface. J Struct Biol. 2003;141(3):208-217.
49. Baig AA, Fox JL, Young RA, et al. Relationships among carbonated apatite solubility, crystallite size, and microstrain parameters. Calcif Tissue Int. 1999;64(5):437-449.
50. Ibsen CJS, Chernyshov D, Birkedal H. Apatite formation from amorphous calcium phosphate and mixed amorphous calcium phosphate/amorphous calcium carbonate. Chemistry. 2016;22(35):12347-12357.
51. Burr DB. Changes in bone matrix properties with aging. Bone. 2019;120:85-93. https://doi.org/10.1016/j.bone.2018.10.010.
52. Mow VC, Ratcliffe A, Robin PA. Cartilage and diarthrodial joints as paradigms for hierarchical materials and structures. Biomaterials. 1992;13(2):67-97.
53. Kirsch T. Determinants of pathological mineralization. Curr Opin Rheumatol. 2006;18(2):174-180.
54. Ho AM, Johnson MD, Kingsley DM. Role of the mouse ank gene in control of tissue calcification and arthritis. Science. 2000;289(5477):265-270.
55. Reznikov N, Steele JAM, Fratzl P, Stevens MM. A materials science vision of extracellular matrix mineralization. Nat Rev Mater. 2016;1(8):16041.
56. Bertrand J, Nitschke Y, Fuerst M, et al. Decreased levels of nucleotide pyrophosphatase phosphodiesterase 1 are associated with cartilage calcification in osteoarthritis and trigger osteoarthritic changes in mice. Ann Rheum Dis. 2012;71(7):1249-1253. https://doi.org/10.1136/annrheumdis-2011-200892.
57. Fawns HT, Landells JW. Histochemical studies of rheumatic conditions. I. Observations on the fine structures of the matrix of normal bone and cartilage. Ann Rheum Dis. 1953;12(2):105-113.
58. Lane LB, Bullough PG. Age-related changes in the thickness of the calcified zone and the number of tidemarks in adult human articular cartilage. J Bone Joint Surg Br. 1980;62(3):372-375.
59. O'Connor KM. Unweighting accelerates tidemark advancement in articular cartilage at the knee joint of rats. J Bone Miner Res. 1997;12(4):580-589.
60. Doube M, Firth EC, Boyde A. Variations in articular calcified cartilage by site and exercise in the 18-month-old equine distal metacarpal condyle. Osteoarthritis Cartilage. 2007;15(11):1283-1292.
61. Lemperg R. The subchondral bone plate of the femoral head in adult rabbits. Virchows Arch A Pathol Pathol Anat. 1971;352(1):1-13. https://doi.org/10.1007/BF00549758.
62. Green WTJ, Martin GN, Eanes ED, Sokoloff L. Microradiographic study of the calcified layer of articular cartilage. Arch Pathol. 1970;90(2):151-158.
63. Gerber HP, Vu TH, Ryan AM, Kowalski J, Werb Z, Ferrara N. VEGF couples hypertrophic cartilage remodeling, ossification and angiogenesis during endochondral bone formation. Nat Med. 1999;5(6):623-628.
64. Cox LGE, van Donkelaar CC, van Rietbergen B, Emans PJ, Ito K. Alterations to the subchondral bone architecture during osteoarthritis: bone adaptation vs endochondral bone formation. Osteoarthritis Cartilage. 2013;21(2):331-338. https://doi.org/10.1016/j.joca.2012.10.013.
65. van der Kraan PM, Stoop R, Meijers THM, Poole AR, van den Berg WB. Expression of type X collagen in young and old C57Bl/6 and Balb/c mice. Relation with articular cartilage degeneration. Osteoarthritis Cartilage. 2001;9(2):92-100.
66. Glimcher MJ. Bone: nature of the calcium phosphate crystals and cellular, structural, and physical chemical mechanisms in their formation. Rev Mineral Geochem. 2006;64(1):223-282.
67. Aghajanian P, Mohan S. The art of building bone: emerging role of chondrocyte-to-osteoblast transdifferentiation in endochondral ossification. Bone Res. 2018;6(1):19. https://doi.org/10.1038/s41413-018-0021-z.
68. Zhou X, von der Mark K, Henry S, Norton W, Adams H, de Crombrugghe B. Chondrocytes transdifferentiate into osteoblasts in endochondral bone during development, postnatal growth and fracture healing in mice. PLoS Genet. 2014;10(12):e1004820.
69. Yang L, Tsang KY, Tang HC, Chan D, Cheah KSE. Hypertrophic chondrocytes can become osteoblasts and osteocytes in endochondral bone formation. Proc Natl Acad Sci U S A. 2014;111(33):12097-12102.
70. Sharma L. The role of varus and valgus alignment in knee osteoarthritis. Arthritis Rheum. 2007;56(4):1044-1047.
71. Moisio K, Chang A, Eckstein F, et al. Varus-valgus alignment reduced risk of subsequent cartilage loss in the less loaded compartment. Arthritis Rheum. 2011;63(4):1002-1009.
72. Sharma L, Jing S, Dunlop D, Felson D, Lynch J, Nevitt M. Varus and valgus alignment and incident and progressive knee osteoarthritis. Bone. 2011;23(1):1-7.
73. Kumar D, Manal KT, Rudolph KS. Knee joint loading during gait in healthy controls and individuals with knee osteoarthritis. Osteoarthritis Cartilage. 2013;21(2):298-305. https://doi.org/10.1016/j.joca.2012.11.008.
74. Cowin SC, Moss-Salentijn L, Moss ML. Candidates for the Mechanosensory system in bone. J Biomech Eng. 1991;113(2):191-197. https://doi.org/10.1115/1.2891234.
75. Klein-Nulend J, Nijweide PJ, Burger EH. Osteocyte and bone structure. Curr Osteoporos Rep. 2003;1(1):5-10.
76. Guilak F. Biomechanical factors in osteoarthritis. Best Pract Res Clin Rheumatol. 2011;25(6):815-823. https://doi.org/10.1016/j.berh.2011.11.013.